Journal of Electroanalytical Chemistry 816 (2018) 99–106

Contents lists available at ScienceDirect

Journal of Electroanalytical Chemistry

journal homepage: www.elsevier.com/locate/jelechem

Review

Functionalized crown ether assisted morphological tuning of CuO nanosheets for electrochemical supercapacitors

S.D. Jagadale[a,*], A.M. Teli[b], S.V. Kalake[a], A.D. Sawant[c], A.A. Yadav[d], P.S. Patil[b]

[a] School of Nanoscience and Technology, Shivaji University, Kolhapur, Maharashtra 416004, India
[b] Thin Film Materials Laboratory, Department of Physics, Shivaji University, Kolhapur, Maharashtra 416004, India
[c] Thin Film Physics Laboratory, Department of Physics, Electronics and Photonics, Rajashri Shahu Mahavidyalaya, Latur, Maharashtra 413512, India
[d] Department of Chemistry, Sanjay Ghodawat University, Kolhapur, Maharashtra 416118, India

ARTICLE INFO

Keywords:
Crown ether
CuO nanosheets
Supercapacitor
Hydrothermal

ABSTRACT

Controlling surface morphology of transition metal oxides play a key role in various applications. Here, we report new and facile route of dibenzothiazolyl dibenzo-18-crown-6 ether (DDCE) assisted synthesis of CuO nanosheets by hydrothermal method. DDCE is used as task specific structure directing agent for the shape controlled synthesis of CuO nanosheets. The effect of DDCE on morphology, surface area and electrochemical properties of CuO nanosheets is studied. The synthesized CuO nanosheets exhibited excellent capacitive properties such as high specific capacitance 130.6 F g^{-1} at 10 mV s^{-1}. These CuO nanosheets play important role in ion transportation and provide more active sites for electrochemical reactions. This work represents a new approach for preparation of CuO nanostructures by hydrothermal method. The prepared CuO nanostructures can be potential electrode material for high performance supercapacitors for the next generation energy storage devices.

1. Introduction

In light of increasing global population and successive rapid industrialization, there is urgent need of adapting new technologies in energy harvesting, storage and conservation. Technology that can produce a compact and reliable energy storage device has utmost commercial importance. To meet ever growing energy demands, energy storage systems such as batteries, fuel cells and supercapacitor technologies are being adapted [1]. Among all of this energy storage devises supercapacitor has its own reward of high efficiency and fast charging discharging cycle. In contrast to batteries, supercapacitors show excellent power density and stability but poor energy density. Therefore, supercapacitors with enhanced energy density will have commercial importance [2–4]. Recently, focused efforts have been made for developing nanostructured electrode materials with improved specific capacitance, increasing the operating voltage and low cost for a supercapacitor application. Charge storage mechanism and type of application are the key aspects in the selection of proper electrode material. Depending on the charge storage mechanism supercapacitors are classified into two major types viz. a) Electric double layer capacitor (EDLC), where charge is stored through electric double layer in carbon based materials and their hybrids [5,6] and b) Pseudocapacitor, where charge is stored Faradically in metal oxides and conducting polymers [7,8]. Because of relatively low specific capacitance of EDLC, pseudocapacitors have engrossed great demand. Most of the transition metal oxides exhibit high specific capacitance and cyclic stability than conducting polymer, therefore they are widely used as electrode material in high performance supercapacitors [9]. Among the metal oxides, CuO as mesoporous electrode materials have attracted enormous attention because of its abundance, non-toxicity, low cost and favourable pseudo capacitive behaviour [10,11]. Recently some research groups have reported different CuO nanostructures for supercapacitor applications. Zhang et al. have synthesized cauliflower like CuO nanostructures by chemical deposition method [12]. This material displayed specific capacitance 116.9 F g^{-1}. Patake et al. reported synthesis of porous and amorphous CuO thin films by electrode deposition method that displayed specific capacitance of 36 F g^{-1} [13], while Dubal et al. [14] developed copper oxide nanosheets by chemical bath deposition and found capacitance 43 F g^{-1} at 10 mV s^{-1}. Nawathe and coworkers reported 3-(10-hydroxypropyl)-1-methylimidazolium chloride[HPMIM][Cl] ionic liquid as electrolyte to check electrochemical properties of nanostructured copper oxide [10]. This material exhibited specific capacitance of 60 F g^{-1}. Recently, 3D porous gear like CuO has been reported on Cu substrate with a specific capacitance of 348 F g^{-1} [15].

* Corresponding author.
E-mail address: surybala_7@yahoo.co.in (S.D. Jagadale).

https://doi.org/10.1016/j.jelechem.2018.01.059
Received 10 September 2017; Received in revised form 11 January 2018; Accepted 31 January 2018
Available online 02 February 2018

Mesoporous CuO nanoribbons have been prepared in the presence of tetraoctyl ammonium bromide (TOAB) with a specific capacitance of 137 F g^{-1} [16]. Also, diverse CuO nanosheets were prepared by wet chemical method and used for supercapacitor application. Synthesized CuO nanosheets exhibited specific capacitance of 88.5 F g^{-1} at the scan rate 2 mV s^{-1} in aqueous 6 M KOH electrolyte [17]. Lokhande et al. designed CuO nanosheets, micro-roses and micro-woollen by chemical bath deposition method, exhibited specific capacitance 303 F g^{-1}, 279 F g^{-1} and 346 F g^{-1} at 5 mV s^{-1} scan rate respectively [18]. Also, CuO nanoflowers synthesized by chemical bath deposition method exhibited specific capacitance about 498 F g^{-1} at the 5 mV s^{-1} in KOH electrolyte [19].

Even though CuO is showing potential supercapacitor applications, the specific capacitance of CuO is still much lower among the other transition metal oxides. To improve the capacitance, there is need to increase the open nanoscale porosity and number of active sites in CuO nanostructures that can provide superior accessibility for electron/ion adsorption and transportation during reversible redox reaction process [20]. Template assisted synthesis provides unique nanostructures with potential applications in energy storage and conversion technology. By template assisted synthesis, it is possible to prepare nanostructured CuO with small crystallite size and large surface area [21]. Silica, tetraoctylammonium bromide, carbon nanotubes and many other materials are reported as template for the synthesis of nanostructured CuO electrode material for supercapacitor application [21–24]. Herein, we report for the first time, DDCE template assisted synthesis of CuO nanosheets by hydrothermal approach. The synthesized CuO exhibited high specific capacitance 130.6 F g^{-1} at 10 mV s^{-1} with 1 M aq. KOH electrolyte.

2. Experimental details

2.1. Synthesis and characterization of CuO electrodes

Dibenzothiazolyl dibenzo-18-crown-6 (DDCE) was used as template for the synthesis of highly ordered CuO nanosheets. This template was prepared by previously reported procedure [25]. The typical procedure of synthesis of DDCE involves two steps as mentioned in Scheme 1. In first step, a mixture of dibenzo-18-crown-6 (2.016 g, 5.6 mmol), trifluoroacetic acid (8.3 mL) and hexamethylenetetramine (3.22 g, 22 mmol) was stirred for 24 h at 90 °C under inert atmosphere of nitrogen. The reaction mixture was extracted with benzene and the extract was dried on magnesium sulphate. Solvent was evaporated under vacuum to get yellow oil, which on cooling solidified to brown crystals of diformyldibenzo-18-crown-6 (2). In second step, diformyldibenzo-18-crown-6 (0.108 g, 0.2 mmol) and 2-aminobenzenethiol (1.52 g, 0.6 mmol) were dissolved in methanol (8 mL). The mixture was refluxed for 24 h with stirring. The reaction mixture was cooled to room temperature and poured on ice to get solid product. The product was filtered and recrystallized in ethanol to get pure DDCE (3). This prepared DDCE was used as structure directing agent for synthesis of nanostructured CuO. For hydrothermal treatment, 50 ml of 0.04 M $CuSO_4$ solution was prepared in deionized water. 10 vol% ammonia was added drop wise in this solution until the solution becomes clear. 1 ml of 0.005 M DDCE solution in ethanol was added to this clear solution and the resulting mixture was stirred at 60 °C for 5 min. A stainless-steel substrate (2 cm × 1 cm) was immersed in this solution bath and then bath was kept in autoclave at 90 °C for 5 min. After cooling the solution to room temperature, the substrate was removed from autoclave, rinsed thoroughly using deionized water and kept at room temperature for air drying. Thus obtained CuO thin film was marked as CuO:CE05. Similarly films were prepared using 0.01 M and 0.015 M of DDCE and these thin films were designated as CuO:CE1 and CuO:CE15 respectively. The mass of active material was calculated from weight difference between the weight of substrate before deposition and weight of the substrate after deposition. The CuO thin films without DDCE were indicated as CuO.

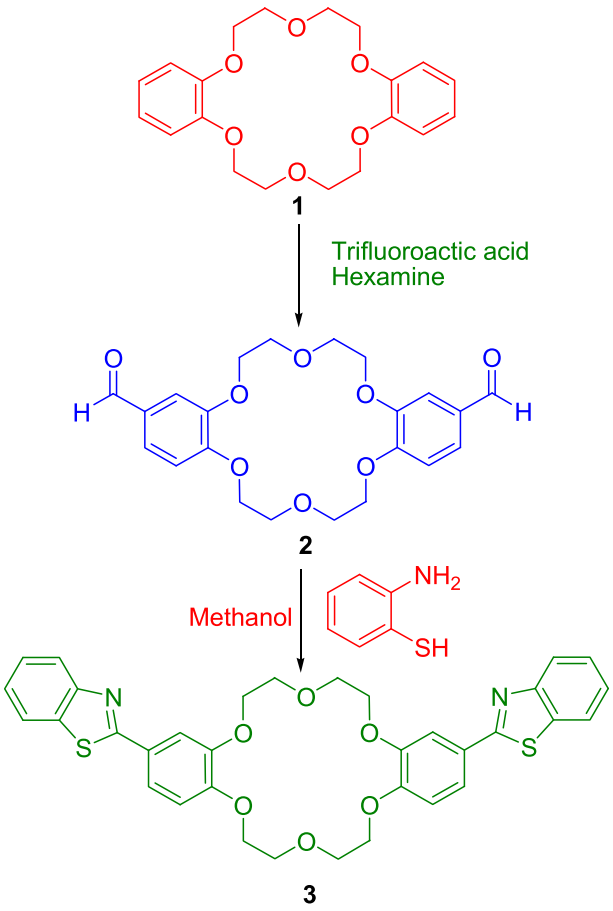

Scheme 1. Synthesis of Dibenzothiazolyldibenzo-18-crown-6-ether.

2.2. Characterization of CuO electrodes

The crystal structures of CuO nanosheets were characterized by X-ray diffraction spectra (Bruker AXS Analytical Instruments Pvt. Ltd., Germany, Model: D2 phaser). The surface morphology of CuO nanosheets was studied using a scanning electron microscope (Model JEOL-JSM-6360, Japan), operated at an acceleration voltage 20 kV. The energy dispersive X- ray spectroscopy (EDAX) was carried out to check elements present in CuO nanosheets by using Oxford instruments INCA with FESEM S4800, Hitachi. The chemical states of the elements were determined by X-ray photoelectron spectroscopy on a Sigma Probe instrument (Thermo Fisher Scientific). Surface area analysis was carried out by Brunauer–Emmett–Teller (BET) nitrogen adsorption/desorption method, at liquid nitrogen temperatures, using N_2 gas as an absorbent (Quantachrome NOVA 1000e, India).

2.3. Electrochemical measurements of CuO electrodes

The prepared CuO electrodes used as working electrodes in a three electrode system with platinum as counter electrode and saturated calomel electrode (SCE) serving as the reference electrode. The electrochemical measurements were performed in 1 M aq. KOH electrolyte using scanning potentiostat (model-CHI-400A) CH Instrument, USA. The charge–discharge and electrochemical impedance spectroscopy (EIS) study was carried out using Wonatech WMPG 1000-potentiostat-Galvanostat.

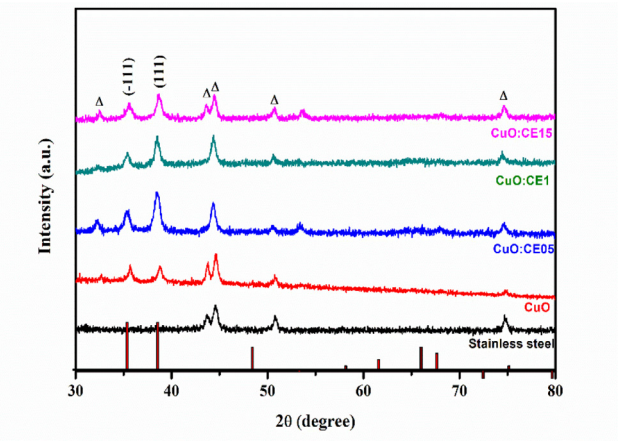

Fig. 1. XRD pattern of CuO nanosheets with and without DDCE.

3. Results and discussion

3.1. Synthesis and characterization of CuO electrodes

3.1.1. X-ray diffraction studies

The X – ray diffraction images of CuO nanosheets with and without DDCE are shown in Fig. 1. The peaks at 35.61° and 38.48° corresponds to (−111) and (111) planes in CuO and CuO:CE samples. All these XRD peak values compared with standard ICDD card (96-101-1149) indicate the formation of monoclinic CuO. The peaks of stainless steel substrate indicated as Δ. The broadening of XRD peaks indicates nanocrystalline nature of CuO nanosheets. The XRD peak (111) slightly dominant than (−111) peak in all CuO nanosheets. With increasing concentration of DDCE, the intensity of (111) peak in CuO nanosheets goes on decreasing. This can be attributed to the fact that intensity of (111) peak in CuO:CE nanosheets decreased with decrease in thick film formation. The diffraction pattern indicates the formation of pure CuO nanosheets, it does not show any other impurity peaks. Furthermore, no carbon peaks were observed in EDAX spectrum indicating complete removal of crown ether.

3.1.2. Scanning electron microscopy

Fig. 2 shows SEM images of CuO nanosheets prepared with and without DDCE. All CuO nanosheets have a smooth, uniform, dense and homogeneous surface morphology without holes and cracks. These images confirm the formation of large number of highly ordered nanosheets. The SEM image of CuO prepared without template (Fig. 2a) consists of densely packed nanosheets. In contrast images of CuO prepared using DDCE (Fig. 2b to d) indicates that relatively loosely packed large number of nanosheets are formed. It is clearly seen that, CuO:CE1 sample has nanosheets with large interlayer spacing which provides more intercalation of ion transportation during redox reaction as compared to CuO:CE05 and CuO:CE15 (Fig. 2b and d). Fig. 2c indicates relatively large number of loosely packed nanosheets, grown almost parallel to each other and provide abundant space for easy access for ion transport. When DDCE was used as template, initially aqueous solution of Cu^{2+} ions and NH_3 leads to nucleation to form CuO nucleus. We propose that, when CuO particles reach to critical size, DDCE absorbs CuO molecules and acts as template to form CuO nanosheets. After electrochemical characterization it was found that CuO:CE1 nanosheets showed maximum specific capacitance 130.6 $F\,g^{-1}$ at 10 $mV\,s^{-1}$. This can be correlated with SEM image of CuO:CE1 sample (Fig. 2c) which indicates existence of large interlayer spacing. This prompted us compare the results of CuO and CuO:CE1 samples to study the effect of DDCE on CuO morphology.

3.1.3. Energy dispersive X- ray spectroscopy

Elemental composition of synthesized CuO and CuO:CE1 nanosheets was determined by EDAX (Fig. 3) which confirms the presence of copper and oxygen in both samples. The absence of carbon peak confirms that there was complete removal of DDCE. This supports our claim that DDCE acts only as structure directing agent.

3.1.4. X-ray photoelectron spectroscopy

The XPS of Cu2p core level for CuO nanosheets showed in Fig. 4.

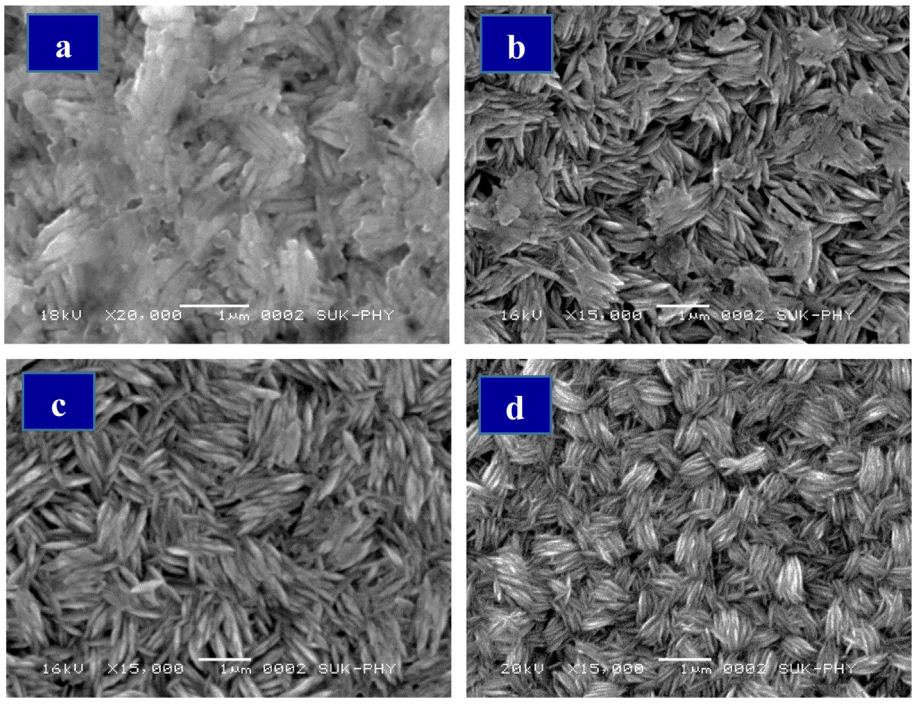

Fig. 2. SEM images of CuO nanosheets a) CuO b) CuO:CE05 c) CuO:CE1 (d) CuO:CE15.

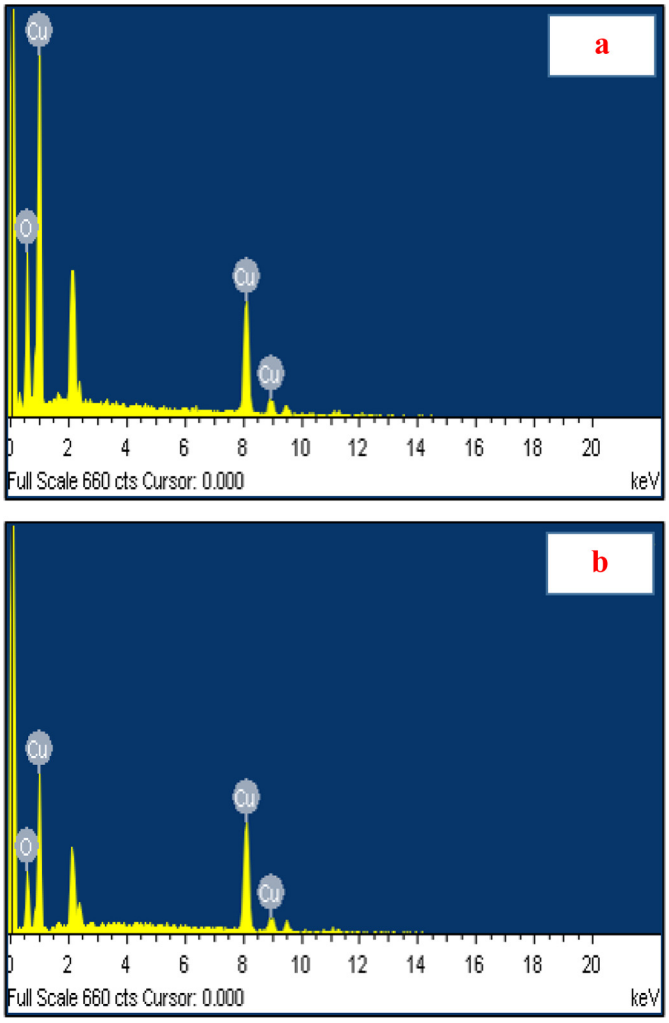

Fig. 3. EDAX spectra of (a) CuO (b) CuO:CE1 nanosheets.

The binding energy of $Cu2p_{3/2}$ and $Cu2p_{1/2}$ for CuO observed at 935 eV and 954.6 eV and for CuO:CE1 at 934.8 eV and 954.5 eV respectively. These values indicate the presence of Cu^{2+} in the sample. Also, two shake up peaks are observed at 943 eV and 962 eV which are at higher level than corresponding main peaks. This confirms presence of unfilled $Cu3d^9$ shell. This implies the presence of copper in +2 oxidation state. The spin orbital difference of 19 eV reveals the formation of CuO.

3.1.5. BET surface area

The specific surface area of CuO and CuO:CE1 nanosheets was determined by nitrogen adsorption and desorption measurements as shown in Fig. 5. The specific surface area was calculated by applying Brunaer Emmet Tellar (BET) method and pore size distribution were obtained by Barret-Joyner-Halenda (BJH) equation. The adsorption and desorption curve of both samples can be classified as a type IV isotherm with H3 hysteresis. The BET surface area of CuO and CuO:CE1 nanosheets was found to be 6.33 $m^2 g^{-1}$ and 22.93 $m^2 g^{-1}$ respectively. The presence of type IV isotherm with H3 hysteresis loop confirms the formation of mesoporous material.

In the BJH analysis a pore size distribution of 4.79 nm and 3.39 nm for CuO and CuO:CE1 samples was observed. These results revealed that, the difference in the surface areas of the CuO nanosheets with and without DDCE resulted due to great difference in their surface morphologies. These hierarchical surface morphologies with fine pores are favourable for easy intercalation of electrolyte ions within the pores that can help in increasing the specific capacitance.

3.1.6. Role of DDCE

As a matter of choice, we selected functionalized crown ether, DDCE prepared previously in our laboratory [25]. This crown ether has cavity with additional binding sites of hetero atoms such as nitrogen and sulphur. So also, it is soluble in aqueous solutions and decomposes above 85 °C making it compatible for aqueous hydrothermal process. This task specific functionalized crown ether acts as structure directing agent in crystal growth of CuO to form different morphology. Based on properties of DDCE and post synthesis ^{13}C NMR analysis, a mechanism for DDCE assisted synthesis of nanostructured CuO sheets is proposed. Here, DDCE acts as a structure directing agent. We propose that, CuO nucleate to form nano sized particles as shown in Fig. 6. This process subsequently aggregate nanosheets on the substrates. The plausible chemical reactions in the synthesis of CuO nanostheets can be represented as below.

$$CuSO_4 + 2NH_3(aq) + 2H_2O \rightarrow Cu(OH)_2 + (NH_4)_2SO_4 \quad (1)$$

$$Cu(OH)_2 \rightarrow CuO + H_2O \quad (2)$$

It is reported that capping agent play important role in substrate binding process and crystal growth direction [21–24]. It is observed that DDCE do not take part in the reaction and it only acts as structure directing agent. DDCE is a type of crown ether that has unique ability of binding selective ions or molecules [25]. Therefore, we hypothesized that DDCE can keep molecular level control during synthesis of CuO nanosheets as shown in Fig. 6.

3.2. Electrochemical properties of CuO nanosheets

To test the electrochemical properties of CuO nanosheets cyclic voltametry (CV), Galvanostatic charge discharge (CD) and electrochemical impedance spectroscopy (EIS) analysis was carried out using three electrode system in 1 M aq. KOH electrolyte.

3.2.1. Cyclic voltametry

The CV of CuO and CuO:CE1 nanostructured electrodes at 10 mV s^{-1} in 1 M aq. KOH is shown in Fig. 7. The presence of two quasi reversible electron transfers in curves indicates capacity results from pseudocapacitive capacitance. The shapes of CV reveal that it is very distinct from that of electric double layer capacitor. The CV curves of CuO:CE1 were recorded at different scan rates and are as shown in Fig. 8. The current density increases with increasing scan rate from 10 to 100 mV s^{-1}. With increasing scan rate, the area under the curve go on increasing and also anodic and cathodic peak potential shift in more anodic and cathodic directions respectively. There is a continuous decrease in the specific capacitance with an increase in scan rate. The decrease in capacitance is attributed to the presence of inner active sites that cannot sustain the redox transitions at higher scan rates. This is probably due to the diffusion effect of protons within the electrode. Specific capacitance of CuO samples were calculated by using the equation as below:

$$Csp = \frac{\int idV}{2m\Delta VS} \quad (3)$$

where, $\int idV$ is area under the curve, ΔV is potential range (V), m is active mass loaded on stainless steel substrate (g) and S is scan rate (mV s^{-1}).

The decrease in capacitance suggests that at high scan rates all the active species of the electrode are not able to take part in the charge

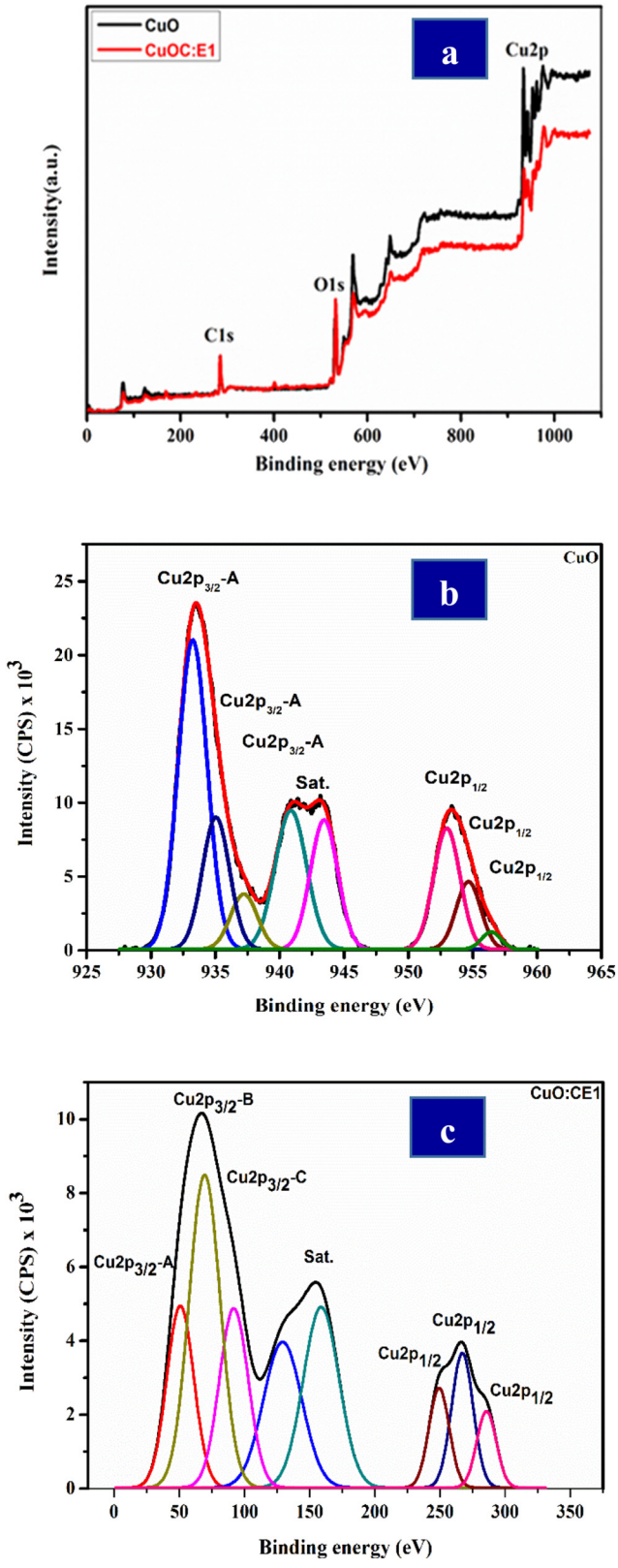

Fig. 4. (a) Full XPS spectra of CuO and CuO:CE1 nanosheets. (b) and (c) Core level Cu2p spectra of CuO and CuO:CE1 respectively.

storage process. Hence, the specific capacitance obtained at a slow scan rate could be considered for the full utilization of electrode material. The specific capacitance of CuO and CuO:CE1 were 48.4 and 130.6 F g^{-1} in 1 M aq. KOH at 10 mV s^{-1} (Table 1). (See Table 2.)

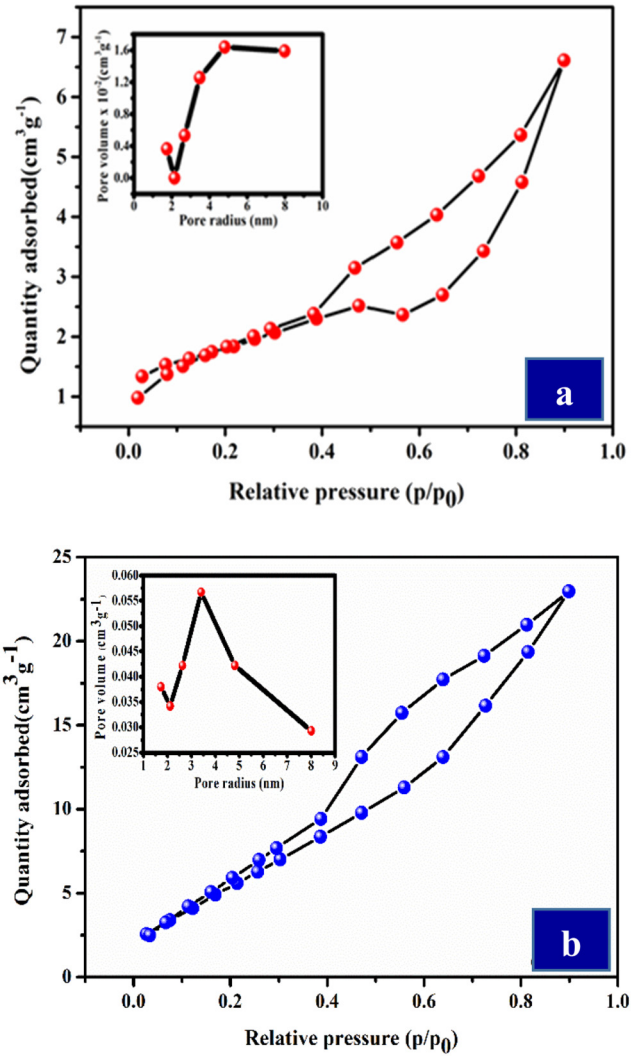

Fig. 5. Nitrogen adsorption and desorption isotherms and corresponding (BJH) pore size distribution curves for (a) CuO and (b) CuO:CE1 nanosheets.

3.2.2. Galvanostatic charge-discharge

Fig. 9 shows the Galvanostatic charge discharge curves for CuO and CuO:CE1 nanosheets at 1 mA cm^{-2} within potential range 0 V to 0.5 V in 1 M aq. KOH as electrolyte. It was found that there is saturation of current after 0.5 V for CuO sample. Voltage range for CuO:CE1 decreased below 0.5 V. The non-linear nature of charge discharge curves supported pseudocapacitive behavior of CuO nanosheets [26]. The specific capacitance values from voltage – time measurements calculated by equation below:

$$Csp = \frac{I.\,dT}{m.\,dV} \tag{4}$$

where, I is discharge current (mA) and m is deposited mass (mg), dT is discharge time (s) and dV is potential difference (V).

3.2.3. Electrochemical impedence spectroscopy

Further EIS measurements were carried for CuO and CuO:CE1 nanostructured electrode and resultes are as shown in Fig. 10. The Nyquist plots indicate outstanding electrochemical behaviour of CuO:CE1 electrode. EIS study was carried out at 10 mV s^{-1} in 1 M aq. KOH electrolyte within 10 KHz to 1 KHz frequency range. The Nyquist plot showed two regions, semicircle region at high frequency and straight line at medium or low frequency region. The intercept of the semicircle on real axis at high frequency represents solution resistance (Rs),

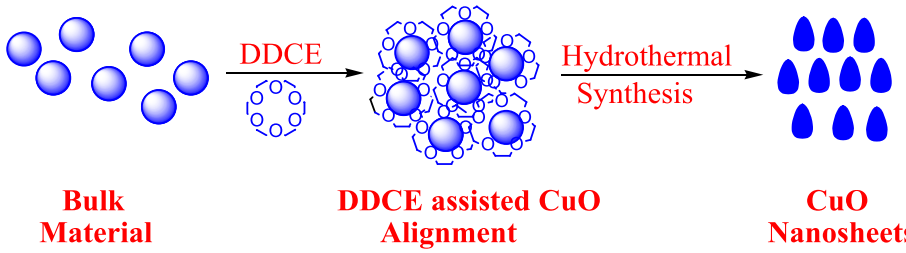

Fig. 6. DDCE assisted alignment of CuO nanosheets by hydrothermal Method.

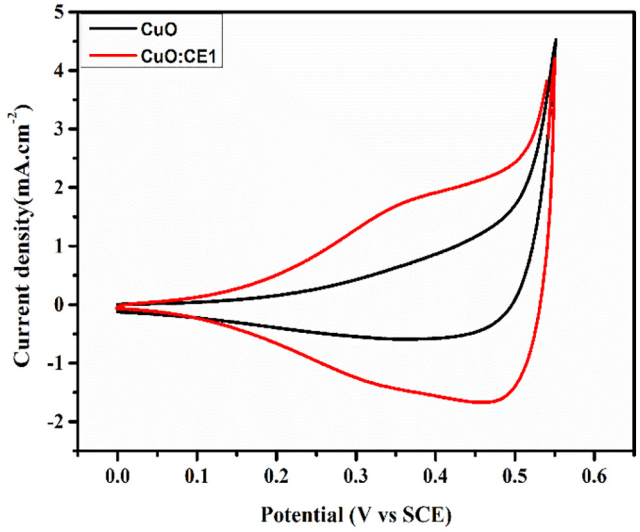

Fig. 7. Cyclic Voltagram curves of CuO and CuO:CE1 at 10 mV s^{-1} scan rate.

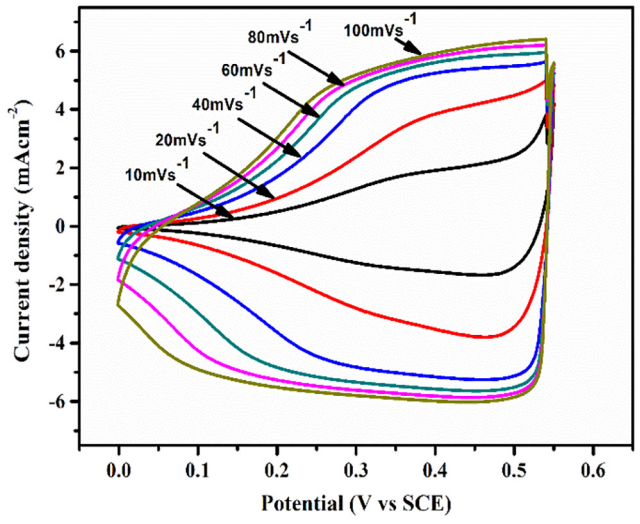

Fig. 8. Cyclic Voltagram of CuO:CE1 at various scan rate.

Table 1
Specific capacitance and mass deposited of different CuO nanosheets.

Sample code	Deposited weight (mg)	Specific capacitance (F g^{-1}) (CV)	Specific capacitance (F g^{-1}) (CD)
CuO	1	48.4	45.7
CuO:CE05	2	74.5	98.6
CuO:CE1	0.8	130.6	232.36
CuO:CE15	0.6	54.8	125.58

Table 2
Specific capacitance of CuO:CE1 nanosheets calculated by CV curves at different scan rate.

Scan rate (mV s^{-1})	Deposited weight (mg)	Specific capacitance (F g^{-1})
10	0.0008	130.6
20	0.0008	133.0
40	0.0008	105.6
60	0.0008	82.6
80	0.0008	67.7
100	0.0008	23.6

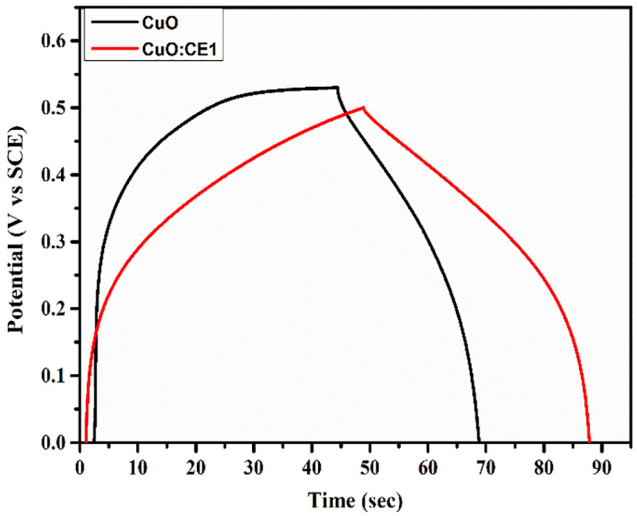

Fig. 9. Galvanostatic charge discharge curves of CuO and CuO:CE1 nanosheets at 1 mA cm^{-2} scan rate.

diameter of semicircle corresponds to the charge transfer resistance (Rct) [27]. The diameter of semicircle corresponds to charge transfer resistance (Rct) caused by Faradic reactions [28], due to Cu^{2+}/Cu^{+} redox couple. The straight line in the medium frequency region due to Warburgimpedance [29], related to the intercalation of electrolyte within the CuO nanostructures.

The series resistance Rs = 2.1 Ω and charge transfer resistance Rct = 36.2 Ω were observed for CuO electrode. CuO:CE1 electrode showed series resistance Rs = 0.24 Ω and charge transfer resistance Rct = 0.23 Ω series which is very less than CuO electrode. CuO:CE1 electrodes exhibit low series resistance Rs and charge transfer resistance Rct, pointing out higher electrical conductivity and high surface area for electrode reactions. Large number of CuO:CE1 nanosheets provide internal accessible surface area due to which more electrolyte penetrate into the sample, reduces internal resistance and enhance electrolytic surface utilization during electrochemical reactions.

Long cyclic stability is also another important property of electrode material. The cyclic performance of CuO and CuO:CE1 electrodes for

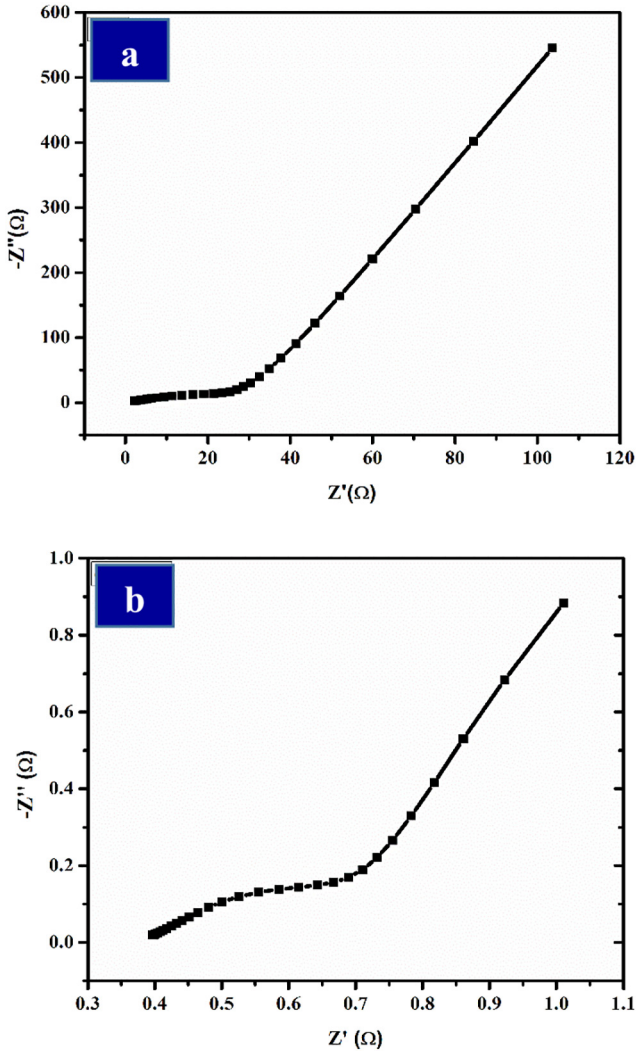

Fig. 10. Electrochemical impedance spectroscopy plot of a) CuO and b) CuO:CE1 nanosheets.

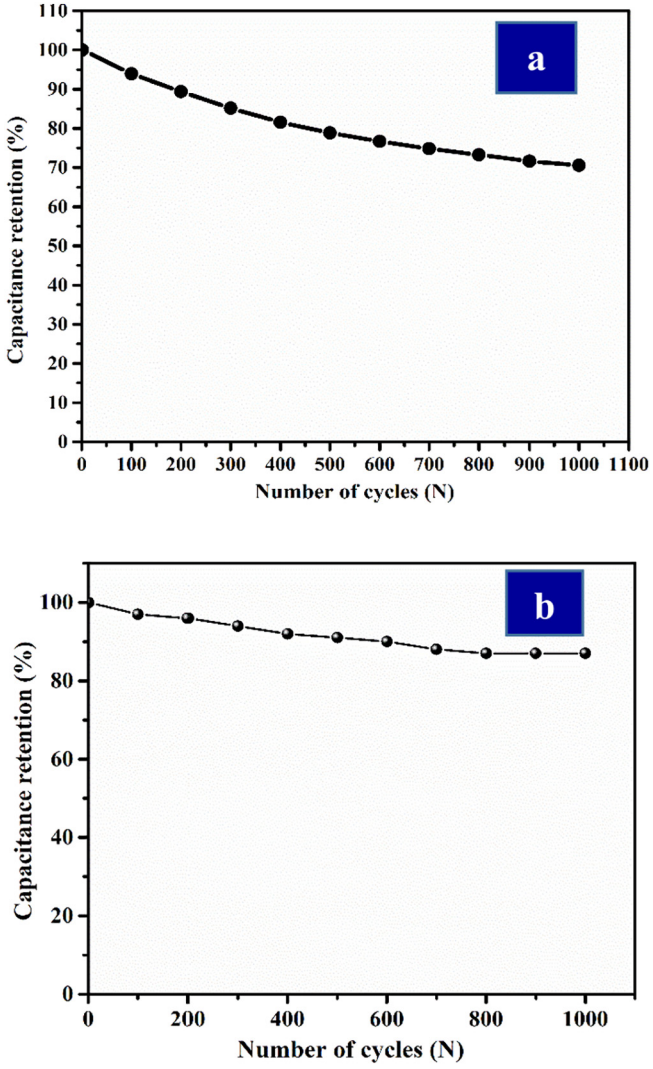

Fig. 11. Stability of a) CuO and b) CuO:CE1 nanosheets for 1000 CV cycles.

1000 cycles shown in Fig. 11. The CuO:CE1 electrode shows superior capacitance retention as compared to CuO electrode. Overall these results demonstrate the high specific capacitance and excellent electrochemical properties of CuO:CE1 nanosheets and thereby making them a promising electrode for supercapacitor application.

4. Conclusions

The results demonstrate synthesis of CuO nanosheets by simple and inexpensive hydrothermal method by using functionalized crown ether, DDCE as a task specific structure directing agent. The crown ether assisted synthesis of CuO nanosheets showed promising improvement in electrochemical properties. The concentration of DDCE has impact on the size, porosity and morphology of material. The synthesized CuO nanosheets are highly ordered nanostructures with high specific surface area and high specific capacitance. Our results indicate that these CuO nanostructures can be used as potential electrode material for various energy devices such as supercapacitor, Li ion batteries, fuel cells and other electronic devises. This work put forth a new way of controlling morphology of materials by preparing task specific functionalized crown ethers. Further investigations are in progress in our laboratory to explore use of functionalized crown ethers in material synthesis.

Acknowledgement

Authors wishes to acknowledge CSIR, New Delhi for financial assistance through major research project (sanction no.03/(1240)/12/EMR-II).

References

[1] M. Winter, R.J. Brodd, Chem. Rev. 104 (2004) 4225.
[2] C. Liu, F. Li, L.P. Ma, H.M. Cheng, Adv. Mater. 22 (2010) E28.
[3] G. Wang, L. Zhang, J. Zhang, Chem. Soc. Rev. 41 (2012) 797.
[4] F.K. Butt, M. Tahir, C. Cao, F. Idrees, R. Ahmed, W.S. Khan, Z. Ali, N. Mahmood, M. Tanveer, A. Mahmood, I. Aslam, ACS Appl. Mater. Interfaces 6 (2014) 13635.
[5] L. Dai, D.W. Chang, J.B. Baek, W. Lu, Small 8 (2012) 1130.
[6] J. Liu, L. Zhang, H.B. Wu, J. Lin, Z. Shen, X.W. Lou, Energy Environ. Sci. 7 (2014) 3709.
[7] S.K. Meher, G.R. Rao, J. Phys. Chem. C 115 (2011) 15646.
[8] K. Liang, X. Tang, W. Hu, J. Mater. Chem. A 22 (2012) 11062.
[9] D. Hulicova-Jurcakova, M. Kodama, S. Shiraishi, H. Hatori, Z.H. Zhu, G.Q. Lu, Adv. Funct. Mater. 19 (2009) 1800.
[10] G.N. Nawathe, D.S. Patil, P.R. Jadhav, D.V. Awale, A.M. Teli, S.C. Bhise, S.S. Kolekar, M.M. Karanjkar, J.H. Kim, P.S. Patil, J. Electroanal. Chem. 738 (2015) 170.
[11] S.M. Pawar, J. Kim, A.I. Inamdar, H. Woo, Y. Jo, B.S. Pawar, S. Cho, H. Kim, H. Im, Sci. Rep. 6 (2016) 21310, , http://dx.doi.org/10.1038/srep21310.
[12] H. Zhang, M. Zhang, Mat, Chem. Phys. 108 (2008) 184.
[13] V.D. Patake, S.S. Joshi, C.D. Lokhande, O.S. Joo, Mater. Chem. Phys. 114 (2009) 6.
[14] D.P. Dubal, D.S. Dhawale, R.R. Salunkhe, V.S. Jamdade, C.D. Lokhande, J. Alloys Compd. 492 (2010) 26.
[15] L. Yu, Y. Jin, L. Li, J. Ma, G. Wang, B. Geng, X. Zhang, Cryst. Eng. Comm. 15 (2013)

7657.
[16] Y.X. Zhang, M. Huang, M. Kuang, C.P. Liu, J.L. Tan, M. Dong, Y. Yuan, X.L. Zhao, Z. Wen, Int. J. Electrochem. Sci. 8 (2013) 1366.
[17] Y.X. Zhang, M. Huang, F. Li, Z.Q. Wen, Int. J. Electrochem. Sci. 8 (2013) 8646.
[18] D.P. Dubal, G.S. Gund, R. Holze, C.D. Lokhande, J. Power Sources 242 (2013) 687.
[19] S.K. Shinde, D.P. Dubal, G.S. Ghodake, V.J. Fulari, RSC Adv. 5 (2015) 4443.
[20] D.P. Dubal, G.S. Gund, R. Holze, H. Jadhav, C.D. Lokhande, C. JinPark, Dalton Trans. 42 (2013) 6459.
[21] Y. Ye, C. Jo, I. Jeong, J. Lee, Nanoscale 5 (2013) 4584.
[22] S.E. Moosavifard, M.F. El-Kady, M.F. Rahmanifar, R.B. Kaner, M.F. Mousavi, ACS Appl. Mater. Interfaces 7 (2015) 4851.
[23] Y. Xin, Y.X. Zhang, M. Huang, M. Kuang, C.P. Liu, J.L. Tan, M. Dong, Y. Yuan, X.L. Zhao, Z. Wen, Int. J. Electrochem. Sci. 8 (2013) 1366.
[24] V. Gupta, N. Miura, Mater. Lett. 60 (2006) 1466.
[25] S.D. Jagadale, A.D. Sawant, M.B. Deshmukh, J. Heterocycl. Chem. 54 (2017) 161.
[26] D. Sarkar, G.G. Khan, A.K. Singh, K. Mandal, J. Phys. Chem. C 117 (2013) 15523.
[27] B. Vidhyadharan, I.I. Misnon, R.A. Aziz, K.P. Padmasree, M.M. Yusoff, R. Jose, J. Mater. Chem. A 2 (2014) 6578.
[28] Q. Li, X.F. Lu, H. Xu, Y.X. Tong, G.R. Li, ACS Appl. Mater. Interfaces 6 (2014) 2726.
[29] A. Pendashteh, M.S. Rahmanifar, R.B. Kaner, M.F. Mousavi, Chem. Commun. 50 (2014) 1972.